



ORIGINAL ARTICLE

Dual recognition strategy for ultra-sensitive fluorescent detection of Hg^{2+} at femto-molar level based on aptamer functionalized sulfur quantum dots



Xiaobin Wang^a, Wei Guo^{b,*}, Xiaoling Wang^a, Qing Hua^a, Feiyan Tang^a, Xin Li^a, Feng Luan^a, Zhiyang Zhang^c, Chunyuan Tian^a, Xuming Zhuang^{a,*}, Lijun Zhao^{a,*}

^a College of Chemistry and Chemical Engineering, Yantai University, Yantai 264005, China

^b Shandong Dyne Marine Biopharmaceutical Co, Ltd, Weihai 264300, China

^c Shandong Key Laboratory of Coastal Environmental Processes, Yantai Institute of Coastal Zone Research, Chinese Academy of Sciences, Yantai 264003, China

Received 21 April 2022; accepted 26 June 2022

Available online 1 July 2022

KEYWORDS

Dual recognition strategy;
Sulfur quantum dots;
Aptamer;
Mercury ions;
Ultrasensitive

Abstract In the present study, a dual recognition strategy for ultrasensitive detection of Hg^{2+} was successfully developed for the first time based on aptamer functionalized sulfur quantum dots (Apt-SQDs). The developed Apt-SQDs not only retained the good fluorescence properties of quantum dots but also overcame the problem of poor selectivity of SQDs for heavy metal ions. This system used the dual recognition strategy, including the combination of S_x^{2-} and Hg^{2+} and T- Hg^{2+} -T structures to excellently identify and capture Hg^{2+} , and an ultrahigh sensitivity fluorescent aptasensor was fabricated. The fluorescent aptasensor had a good response to Hg^{2+} at concentrations ranging of 10^{-15} to 10^{-7} M with an ultralow limit of detection of 0.3 fM, and the response to other metal ions was far less than that to Hg^{2+} . It was successfully applied to detect Hg^{2+} in nearby environmental water samples (tap water, lake water and river water) with a good recovery rate. Moreover, portable test papers that would be useful for Hg^{2+} monitoring in environmental water were designed. The dual recognition strategy not only achieves ultrasensitive fluorescent detection of Hg^{2+} but also provides a new insight into the further expansion of the application of SQDs.

© 2022 The Authors. Published by Elsevier B.V. on behalf of King Saud University. This is an open access article under the CC BY-NC-ND license (<http://creativecommons.org/licenses/by-nc-nd/4.0/>).

* Corresponding authors.

E-mail addresses: guodawei0298@163.com (W. Guo), xmzhuang@iccas.ac.cn (X. Zhuang), zhaoljtu@ytu.edu.cn (L. Zhao).

Peer review under responsibility of King Saud University.



1. Introduction

Heavy metal contamination has always been one of the inevitable problems of human society. Although some heavy metal elements (Cu^{2+} , Zn^{2+} , etc.) (Takeda et al., 2014; Kukic et al., 2014; Han et al., 2017) are essential trace elements for biological activities, most of the heavy metal elements (Morales et al., 2015) cause irreversible damage to organisms, especially the human body (Abraham et al., 2021; Hino et al., 2010; Li et al., 2020a,b). Mercury (Hg^{2+}) is one of the most harmful heavy metal elements. It has been proven to not only display a strong affinity for sulfhydryl groups in the body, allowing it to interact with most sulfhydryl-containing substances, such as proteins and important enzymes involved in the metabolism of substances in the body (cytochrome oxidase (Sugio et al., 2010), succinate dehydrogenase (Tamás and Zelinová, 2017) and lactate dehydrogenase (Ozkan, 2011), and subsequently inactivate the enzyme and harm human health but also cause kidney failure and a variety of neurological symptoms (movement disorders (Taylor et al., 2018), Minamata disease (Eto et al., 2010), etc.). Once Hg^{2+} enters the human body, it is difficult to remove and causes serious damage to the human body. Therefore, timely monitoring of ultratrace Hg^{2+} concentrations in the environment might effectively prevent bioenrichment and avoid eventual entry into the human body. Therefore, the ultrasensitive detection of Hg^{2+} is very important. At present, approaches based on various materials have been developed to detect Hg^{2+} , including electrochemistry (Yerga et al., 2013), electrochemiluminescence (Zhao and Zhou, 2012), surface-enhanced Raman spectroscopy (Li et al., 2018) and fluorescence (Lu et al., 2015) methods, such as Yuan and his coworkers summarized some small molecular fluorescent probes for detection of Hg^{2+} developed in recent years (Yuan et al., 2022). Shellaiah and Sun reviewed metal-organic frameworks used for detecting and removing elemental mercury and Hg^{2+} (Shellaiah and Sun, 2021). Amico and his group studied some research progress using micro extraction techniques in determination of environmental Hg^{2+} (Amico et al., 2022). Daniel and his colleges reported many electrochemical methods for mercury analysis in various samples (Daniel et al., 2013). In particular, the fluorescence method has attracted much attention because of its advantages of high sensitivity, simple operation and a fast detection time. Liu and colleagues designed and developed a highly sensitive fluorescence probe based on anthraquinone derivatives for the detection of Hg^{2+} (Liu et al., 2021a,b,c). Ma and his colleagues efficiently synthesized a novel tetraphenylene-based fluorescence probe based on aggregation-induced emission for the sensitive detection of Hg^{2+} (Ma et al., 2018). In recent years, a fluorescent aptasensor technology developed based on the fluorescence method has gradually attracted the attention of the larger public. Although many sensors based on aptamers have been developed (Tabaraki and Rahmatinya, 2021; Peng et al., 2018a,b), significant challenges remain in the detection of ultratrace Hg^{2+} concentrations.

Fluorescent aptasensors that combine the high specificity of aptamers with the good sensitivity of the fluorescence method exhibit good analytical performance (Zhou et al., 2019). With aptamers as recognition units and new fluorescent dyes as conversion labeling materials, the sensor further develops in the direction of less sample consumption, high specificity and sensitivity, a fast response speed and short reaction time, playing an increasingly important role in life science detection (Hassan and Derosa, 2020), food safety (Guo et al., 2014) and environmental monitoring (Peng et al., 2018a,b). Chiu and Huang reviewed the recent development of biosensors with functional adaptors and different types of nanomaterials (Chiu and Huang, 2009). Shi and coworkers constructed a fluorescent aptasensor based on aptamer-modified copper@gold nanoclusters to detect Hg^{2+} (Shi et al., 2021). Hu and colleagues constructed an ultrasensitive homogeneous fluorometric assay for Hg^{2+} based on gold nanoparticles and CdTe quantum dots (Hu et al., 2016). Although the performance of these fluorescent aptasensors is good, the difficulties in preparation, significant biotoxicity and high cost of these materials obviously limit their applications. A cheap, easy-to-prepare, low-toxicity and environ-

mentally friendly nanomaterial is needed to construct fluorescent aptasensors.

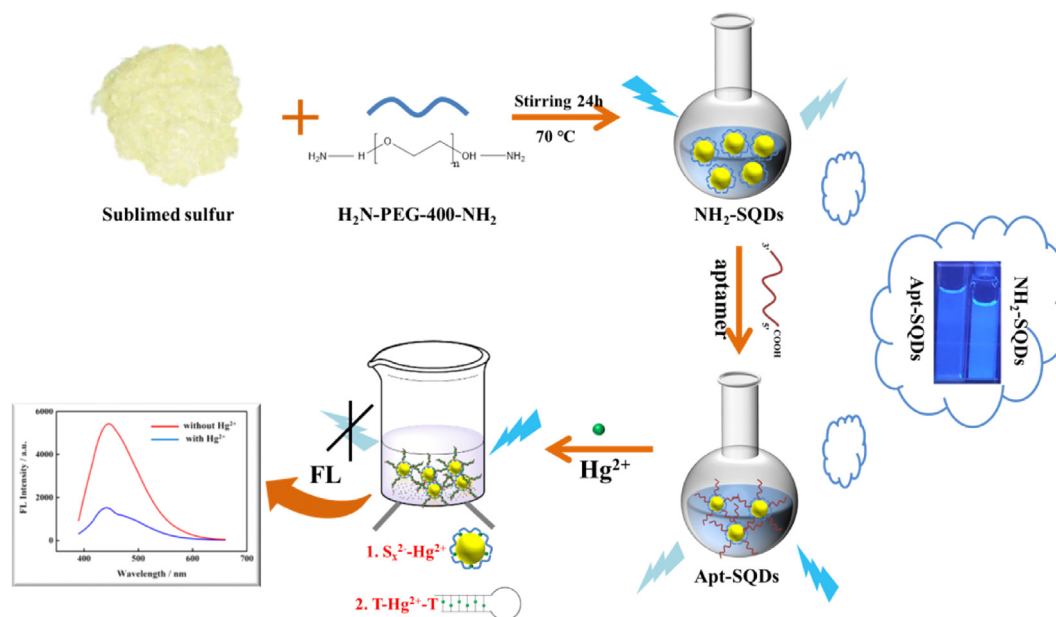
In recent years, sulfur quantum dots (SQDs) have become a new pure element of quantum dot nanomaterials. SQDs not only retain the good optical properties of traditional quantum dots but also overcome potential problems, such as heavy metal pollution, poor biocompatibility and harsh synthetic conditions. Bao and colleagues reported a simple method for the detection of cobalt ions based on SQDs fluorescence quenching (Bao et al., 2019). Chen and colleagues developed a highly sensitive and selective fluorescence sensor for the detection of silver ions (Ag^+) using SQDs (Chen et al., 2016). Fu et al. established an electrochemical sensor for Ag^+ determination based on an SQDs-modified Au electrode (Fu et al., 2020). However, the postsynthetic modification of SQDs synthesized with polyethylene glycol-400 (PEG-400) as a passivator is difficult, and some heavy metal elements easily combine with sulfur ions, which results in limited selectivity of SQDs in heavy metal ion detection. Therefore, using SQDs as a fluorescence probe to detect heavy metal ions has certain limitations, which has hindered the development of Hg^{2+} detection strategies. As a method to solve this problem, an efficient enrichment method for Hg^{2+} based on the thymine- Hg^{2+} -thymine structure (T- Hg^{2+} -T) has attracted widespread attention and become an effective method for the detection of Hg^{2+} . Zhang and his colleagues designed a fluorescence detection method for Hg^{2+} in aqueous solution based on *n*-methyl porphyrin IX/G-quadruple DNA using T- Hg^{2+} -T (Zhang et al., 2017). Shi and his coworkers designed a photochemical method for Hg^{2+} determination based on T- Hg^{2+} -T with double signal amplification (Shi et al., 2017). Xu and colleagues developed a molecular imprinting technology strategy based on T- Hg^{2+} -T to enrich Hg^{2+} in water samples (Xu et al., 2012). Inspired by the studies described above, we intend to combine these two technologies and utilize their synergistic effects to achieve ultrasensitive detection of Hg^{2+} .

In the present study, we improved the synthesis method through the successful postsynthetic modification of SQDs with amino groups (NH_2 -SQDs) and combined these materials with the aptamer of modified carboxyl groups ($-\text{COOH}$) to form the desired fluorescence probe (Apt-SQDs). Combined with the capacity of SQDs to interact with Hg^{2+} and the enrichment function of the T- Hg^{2+} -T structure, an ultrasensitive fluorescent aptasensor was established to detect Hg^{2+} through a dual recognition strategy. The mechanism of the fluorescent aptasensor is shown in Scheme 1. On the one hand, the mechanism is attributed to the strong capacity of S_x^{2-} to bind Hg^{2+} . On the other hand, it is attributed to the effective enrichment of Hg^{2+} by the aptamer. The synergism of the dual recognition strategy may substantially improve the sensitivity of Hg^{2+} detection and achieve the ultrasensitive detection of Hg^{2+} . Benefiting from the selectivity and sensitivity of the developed strategies, the fluorescent aptasensor provided a useful tool for evaluating Hg^{2+} contamination in water samples.

2. Experimental

2.1. Reagents and apparatus

Sublimated sulfur powder, NaOH, 1-(3-dimethylaminopropyl)-3-ethylcarbodiimide hydrochloride (EDC), *N*-hydroxy succinimide (NHS) and Hg^{2+} were purchased from Shanghai Aladdin Biochemical Technology Co., Ltd. (Shanghai, China). Hydrogen peroxide (H_2O_2 , V/V 30%) and other metal ions (Ni^{2+} , Mn^{2+} , Fe^{3+} , Zn^{2+} , Co^{2+} , Cd^{2+} , Pb^{2+} , Cr^{3+} , Cu^{2+} , Al^{3+} , Mg^{2+} and Fe^{2+}) were obtained from Sinopharm Chemical Reagent Co., Ltd. (Tianjin, China). NH_2 -polyethylene glycol-400- NH_2 (NH_2 -PEG-400- NH_2) was synthesized by Huawei Ruike Chemical Co., Ltd. (Beijing, China). Dialysis membranes (1000 Da) were purchased from Shanghai Yuanye Bio-Technology Co., Ltd. (Shanghai, China). All chemicals



Scheme 1 Mechanism of the fluorescent aptasensor based on Apt-SQDs.

were of analytical reagent grade. All the solutions used in this experiment were prepared with ultrapure water (18.2 MΩ cm). The aptamer used in this study was obtained from Sangon Biotechnology Co., Ltd. (Shanghai, China). The base sequence (5-3') of the oligonucleotide was 5-HOOC-(CH₂)₆-TTTTTTTTTTTT-3'.

High-resolution transmission electron microscopy (HR-TEM) images were captured using a JEM-2100F transmission electron microscope at an accelerating voltage of 200 kV (JEOL Ltd, Japan). A Nicolet 5700 Fourier transform infrared (FT-IR) spectrometer (Thermo Electron Corporation, USA) was used to obtain FT-IR spectra. Ultraviolet-visible absorption spectra (UV-vis) were recorded using an A560 ultraviolet-visible spectrometer (AOE Instruments, Shanghai) at a wavelength interval of 2 nm. X-ray photoelectron spectra (XPS) were measured using a Thermo ESCALAB-250 instrument (Thermo Fisher Scientific, USA). The fluorescence emission spectrum was obtained using an F-4700 fluorescence spectrophotometer (HITACHI, Japan). X-ray diffraction spectra (XRD) were measured using a SmartLab3 instrument (Rigaku Corporation, Japan).

2.2. Synthesis of NH₂-SQDs

The NH₂-SQDs was prepared according to a previous report (Wang et al., 2019). Briefly, 3 mL of NH₂-PEG-400-NH₂ and 50 mL of the prepared NaOH solution (0.08 g mL⁻¹) were added to 1.4 g of sublimated sulfur powder and stirred in an oil bath at 70 °C for 24 h. During this period, the color of the solution gradually changed from dark yellow to light yellow, and then 3 mL of H₂O₂ were added to it for etching to prepare NH₂-SQDs with good fluorescence performance. NH₂-SQDs were poured into dialysis membranes (with a molecular weight of 1000 Da) to remove unreacted small molecules, and dialysis was performed for 72 h with a water change every 12 h. Afterward, a light yellow solid was obtained by freeze-drying at -20 °C for 24 h. The synthesized solid NH₂-SQDs were stored at 4 °C until use in subsequent experiments.

2.3. Synthesis of Apt-SQDs

The Apt-SQDs was accomplished using a previously published method (Pasanphan and Chirachanchai, 2008). First, aptamers modified with -COOH (Apt-COOH, 10 mL) were activated by EDC (250 mg) and NHS (120 mg) with stirring for 1.5 h at room temperature to promote a better interaction with NH₂-SQDs. NH₂-SQDs was added and allowed to fully react with the activated -COOH for 2 h at room temperature to obtain Apt-SQDs, which were stored at 4 °C until use in subsequent experiments.

2.4. Fabrication of ultrasensitive fluorescent aptasensors

A series of experiments was designed to explore the sensitivity of the fluorescence sensing platform based on NH₂-SQDs. First, the fluorescence properties of Apt-SQDs were fully measured and compared with those of pure SQDs under the same conditions. Next, different concentrations of Hg²⁺ solutions (10⁻¹⁵ to 10⁻⁷ M) were prepared. Dilute 10 μL of the original Hg²⁺ solution (10⁻³ M) to 100 times (10⁻⁵ M) by adding 990 μL of ultrapure water. According to these steps, the different concentrations of Hg²⁺ that we want could be obtained. But we should ensure that the number of dilutions should be as small as possible to ensure the accuracy of the result. Then, different concentrations of Hg²⁺ solutions were added to the Apt-SQDs in a cuvette, and a fluorescence spectrophotometer was used to record the fluorescence quenching of Apt-SQDs by Hg²⁺.

2.5. Quantum yield (QY) measurement

The QY of SQDs, NH₂-SQDs and Apt-SQDs were determined with reference to quinine sulfate (in 0.1 M H₂SO₄). The calculation of QY is according to the following equation:

$$Q = Q_R \frac{I_{AR}}{I_{RA}} \left(\frac{\eta}{\eta_R} \right)^2$$

where 'Q' refers to the quantum yield, 'I' and 'A' stand for emission intensity and absorbance, respectively. ' η ' is the refractive index of the solvent. The 'R' subscripts represent reference standard ($Q_R = 0.54$).

2.6. Stern-Volmer plot

For fluorescence quenching analysis, a Stern–Volmer plot (F_0/F and $[Q]$ relationship) was used according to the following equation:

$$\frac{F_0}{F} = 1 + K_S[Q]$$

where F_0 and F are the fluorescence intensities in the absence and presence of quencher, respectively, and $[Q]$ is the quencher concentration. The Stern–Volmer constant, K_{SV} , provides a direct measure of the quenching efficiencies and is determined from the linear portion of the Stern–Volmer plot.

2.7. Determination of Hg^{2+} in real samples

Water samples were collected from three different areas in Yantai City to evaluate the performance of the proposed fluorescence sensing platform. The collected samples were incubated for 2 h and then filtered through a 0.45 μm membrane to remove large particles of impurities and suspended solids. After treatment, the samples were stored at 4 $^{\circ}C$ to prevent bacterial growth. After the aforementioned treatment, Hg^{2+} was detected using the ultrasensitive fluorescence sensing platform, and different concentrations of Hg^{2+} were added to the real sample to evaluate the detectability of the fluorescence sensing platform in real samples.

2.8. Preparation of test papers

Because Hg^{2+} exhibits a high level of biological toxicity, an effective and convenient method for monitoring Hg^{2+} concentrations in environmental water samples must be developed. The test paper based on the Apt-SQDs quickly detected trace Hg^{2+} in environmental water samples through colorimetry. According to previous reports (Guo et al., 2020), the filter paper was cut into 1 \times 1.5 cm pieces, which were immersed into the Apt-SQD solution. Then, the filter papers were dried at room temperature. Finally, filter papers were treated with different concentrations of Hg^{2+} and reacted for 5 min. The color changes were recorded by irradiation with a 365 nm UV lamp.

3. Results and discussion

3.1. Characterization of NH_2 -SQDs and Apt-SQDs

The morphology and particle size distribution of the prepared SQDs, NH_2 -SQDs and Apt-SQDs were characterized using HR-TEM. Fig. 1A-C and the insets show the TEM and HR-TEM images of SQDs, NH_2 -SQDs and Apt-SQDs, respectively. The morphologies of the three preparations were highly similar and all of them were spherical with good dispersion, suggesting that the original structure of SQDs was not damaged in the process of functionalization. However, in Fig. 1D-F, SQDs had the smallest particle size (~ 2.5 nm), followed by NH_2 -SQDs (~ 4 nm), and Apt-SQDs had the largest particle size (~ 6 nm), which may be caused by the gradual increase in SQDs functionalization. Fig. S1 showed the dynamic light scattering (DLS) spectra of SQDs, indicating

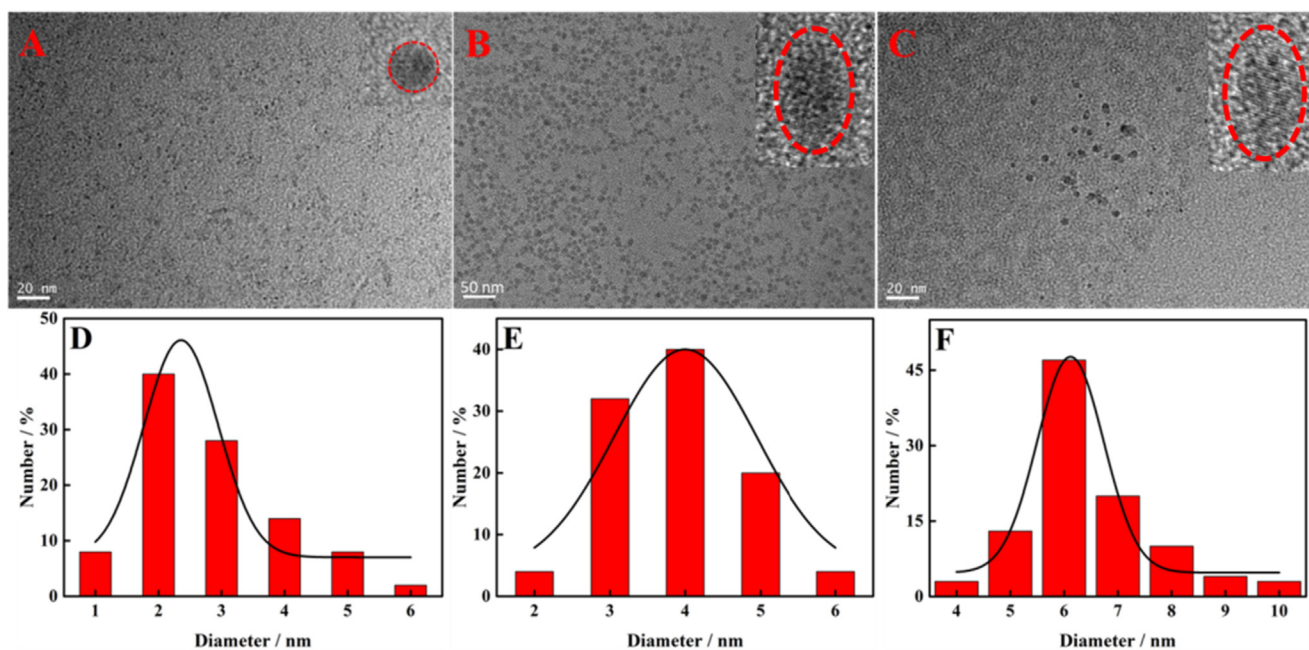


Fig. 1 TEM images of (A) SQDs, (B) NH_2 -SQDs and (C) Apt-SQDs. Insets show HR-TEM images of SQDs, NH_2 -SQDs and Apt-SQDs at 5 nm. Histogram showing the size distribution of (D) SQDs, (E) NH_2 -SQDs and (F) Apt-SQDs.

that the average particle size of prepared SQDs was about 4 nm.

Fig. 2A shows the UV-Vis spectra of SQDs (black curve), NH₂-SQDs (red curve) and Apt-SQDs (blue curve). At 303 nm, all three nanomaterials produced obvious absorption peaks, potentially due to the adsorption of S₂²⁻ on the surface of the SQDs 33. The spectrum (red curve) of NH₂-SQDs was similar to that of SQDs (black curve). However, at approximately 350 nm, NH₂-SQDs produced a small and not obvious absorption peak, which may indicate that other S_x²⁻ molecules were adsorbed on the surface of SQDs during functionalization, similar to the situation reported in the literature³³. However, Apt-SQDs (blue curve) generated a weak absorption peak at 370 nm due to the weak absorption of the carbonyl group of the amide bond and the conjugation of N, and thus we estimated that aptamer had successfully combined with SQDs to generate Apt-SQDs. And the UV-Vis spectra of aptamer was shown in Fig. S2. An obvious absorption peak was observed at 260 nm, which was characteristic of aptamer. In addition, FT-IR spectra of NH₂-SQDs (black curve) and Apt-SQDs (red curve) were recorded to further confirm the successful preparation of Apt-SQDs, as shown in Fig. 2B. Both NH₂-SQDs and Apt-SQDs produced characteristic peaks at 3400 and 2870 cm⁻¹ of SQDs, similar to previous reports (Wang et al., 2019). However, the two nanomaterials showed N-H stretching vibration absorption peaks and N-H bending

vibration peaks at 3300 and 1500 cm⁻¹, respectively, while Apt-SQDs had C=O stretching vibration peaks at 1700 cm⁻¹. Therefore, Apt-SQDs was successfully synthesized and were applied in the next experiment. FT-IR spectra were analyzed to further verify our conclusions, as shown in Fig. S3. Compared with Fig. 2B, characteristic peaks were located at 3300, 2870, 1680 and 1500 cm⁻¹, and characteristic peaks of thymine were located at 3509, 1870, 1196 and 549 cm⁻¹, which was also consistent with a previous report (Bader, 1991), proving that the binding mode of Apt-SQDs to Hg²⁺ was mainly attributed to the T-Hg²⁺-T structure. Fig. 2C and 2D further reveal the composition of Apt-SQDs analyzed using the XPS approach. Fig. 2C shows the presence of mainly four different peaks in the spectrum, indicating that Apt-SQDs mainly contain C, O, N and S. The S peak was selected for further study, and the amplified peak is shown in Fig. 2D. As shown in the figure, the S peak was subdivided into five peaks in the high-resolution XPS spectrum at 161.72, 162.86, 166.86, 168.01 and 169.06 eV. The peaks at 161.72 and 162.86 eV were attributed to S, while the peaks at 166.86 and 168.01 eV were attributed to SO₃²⁻ (2p_{2/3}), and the peak at 169.06 eV was attributed to SO₃²⁻ (2p_{1/2}). Therefore, abundant groups were present on the surface of Apt-SQDs (Wang et al., 2019). The XRD pattern of SQDs presented many sharp peaks, as is shown in Fig. S4, indicating its better crystalline properties, which is similar to previous

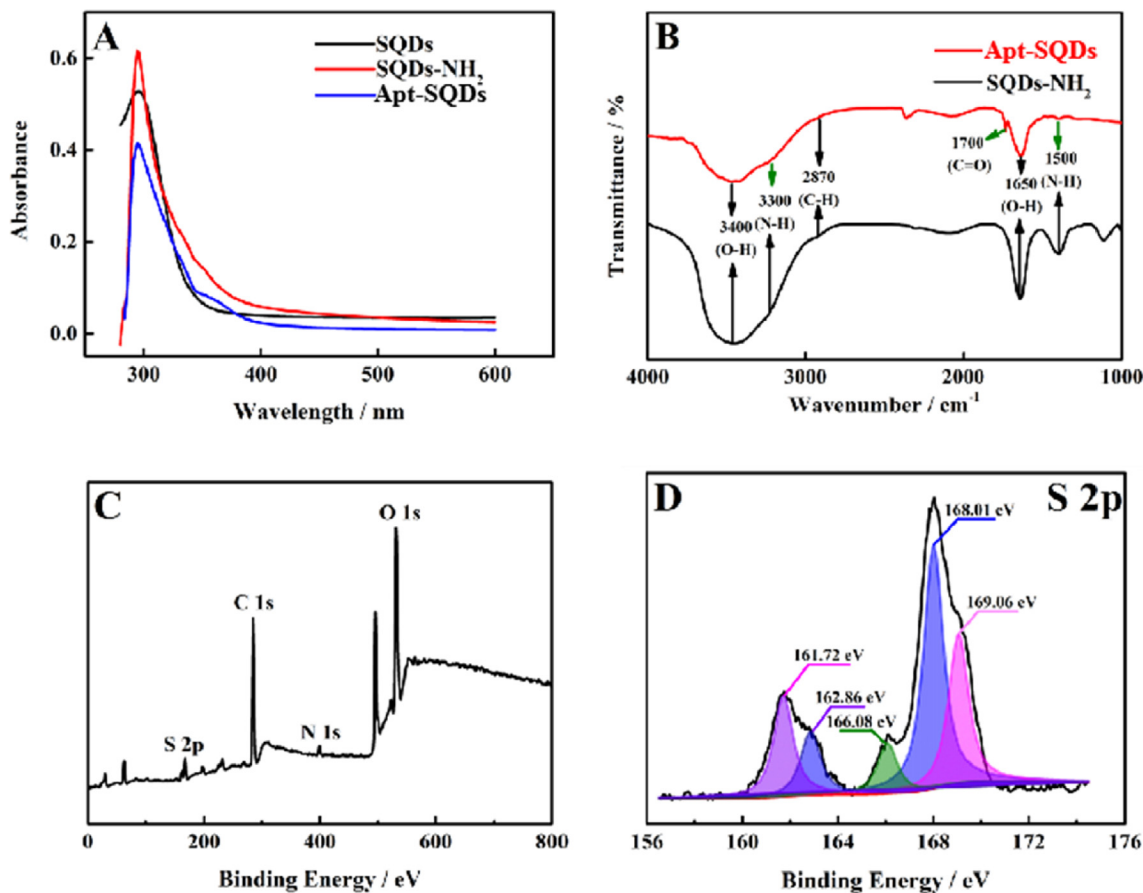


Fig. 2 (A) UV-Vis spectra of SQDs (black curve), NH₂-SQDs (red curve) and Apt-SQDs (blue curve). (B) FT-IR spectra of NH₂-SQDs (black curve) and Apt-SQDs (red curve). (C) XPS survey spectrum and (D) high-resolution S 2p XPS spectrum of NH₂-SQDs.

reports (Chen et al., 2016). The QY of SQDs and Apt-SQDs were 5.3% and 3.4%, respectively, which proves that functionalization has no great impact on SQDs performance. When Hg^{2+} was present, QY of SQDs and Apt-SQDs decreased to 1.4% and 1.1%, respectively, indicating that the prepared material is responsive to Hg^{2+} . The fluorescence lifetime of SQDs and Apt-SQDs were shown in Fig. S5, exhibiting fluorescence lifetime with value of 6.4 ns, which was superior to existing organic fluorophores (generally less than 5 ns). Zeta potential of SQDs, NH_2 -SQDs and Apt-SQDs were shown in Fig. S6. It can be seen that the surface of SQDs have many negative groups. Due to $-\text{NH}_2$ is the electron-donating group, NH_2 -SQDs has a more negative charge on its surface, so the zeta potential of NH_2 -SQDs was more negative than SQDs. As for Apt-SQDs, the aptamer carries more negative charge, which is consistent with the data obtained in Fig. S5 (white column). However, after the addition of Hg^{2+} , the HgS and T-Hg^{2+} -T structure reduces the negative charge on the surface of SQDs, NH_2 -SQDs and Apt-SQDs, so the Zeta potential increases (gray column).

3.2. Quenching mechanism of dual recognition strategy for Hg^{2+}

XPS spectra were recorded to further study the modes of NH_2 -SQDs and Apt-SQDs binding to Hg^{2+} , as shown in Fig. 3. As shown in Fig. 3A-H, the binding modes of NH_2 -SQDs and Apt-SQDs with Hg^{2+} were thoroughly studied. The elemental analysis is shown in Fig. 3A and E, and the SQDs contained Hg, S, C, N and O elements, as expected. Fig. 3B-D shows Hg 4f, S 2p and N 1s spectra, respectively. Fig. 3B shows the XPS spectrum of Hg 4f electrons to reveal the binding modes of NH_2 -SQDs with Hg^{2+} . The peak at 100.9 eV was attributed to HgS . This result indicated that HgS was the main form of Hg binding to NH_2 -SQDs. Fig. 3C shows the spectrum of S 2p electrons. The peak at 161.5 eV was also attributed to HgS , which also proved the conclusion listed above that Hg and NH_2 -SQDs interacted through HgS . Fig. 3F shows the XPS spectrum of Hg 4f electrons to reveal the binding modes of Apt-SQDs with Hg^{2+} . The peak at 100.9 eV in Fig. 3F was much smaller than that in Fig. 3B, which proved that the binding mode of HgS still existed in the interaction of Apt-SQDs and Hg^{2+} , but it was not the main mode. A similar conclusion was drawn from the comparison between the data presented in Fig. 3G and Fig. 3C. The comparison between Fig. 3H and Fig. 3D shows that the peak at 403.4 eV shifted to 401.9 eV, suggesting that the binding mode of Apt-SQDs and Hg^{2+} was indeed different from that of NH_2 -SQDs and Hg^{2+} , which may be caused by the T-Hg^{2+} -T structure.

In order to further proving the quenching mechanism of dual recognition strategy for Hg^{2+} , the FT-IR of aptamer was measured in Fig. S7. Comparing with Fig. S3, it can be seen clearly that it also included N-H stretching vibration absorption peaks, N-H bending vibration peaks and C=O stretching vibration peaks, indicating the adaptor structure was not destroyed during the process of functionalization. However, when the solution exists Hg^{2+} , characteristic peak of aptamer would produce blue shift, attributed to T-Hg^{2+} -T structure.

3.3. Optimizations of conditions

Some optimization experiments were performed to explore the optimal experimental conditions. As shown in Fig. S8A, when Hg^{2+} was added, the fluorescence intensity of Apt-SQDs decreased rapidly, and did not change further after 1 min. Based on this result, Apt-SQDs was useful for Hg^{2+} detection, their response speed to Hg^{2+} detection was extremely fast, and the detection was basically completed within 1 min. The inset showed the quenching of fluorescence intensity in the presence of Hg^{2+} . Fig. S8B shows the results for the detection of Hg^{2+} with Apt-SQDs at different pH values. The fluorescence of Apt-SQDs showed excellent pH stability, and the fluorescence intensity changed by only 5% in the range of pH 4.0–12.0. When Hg^{2+} was added, SQDs showed a good response in the range of pH 6.0–8.0, and 7.0 was selected as the final pH. We speculate that the mechanism of high pH affecting Apt-SQDs fluorescence may be: when pH is too high, Hg^{2+} generates $\text{Hg}(\text{OH})_2$ under alkaline conditions. Due to its low solubility, there is not enough Hg^{2+} in the solution to react with Apt-SQDs. Fig. S8C shows the fluorescence spectra of SQDs with different concentration (10^{-1} , 1, 2, 4, 6, 8 and 10 mg mL^{-1}). It can be seen that with the increase of SQDs concentration, fluorescence intensity increased first and then decreased, and reached the maximum at 1 mg mL^{-1} . The decrease of fluorescence intensity of SQDs at high concentration may be attributed to the fluorescence quenching caused by particle aggregation. The influence of ion strength on SQDs fluorescence intensity was explored, and the results were shown in Fig. S8D. Different concentrations of NaCl (10^{-4} , 10^{-3} , 10^{-2} and 10^{-1} M) was selected as testing reagent. The result shows that within a certain range of ionic strength, the fluorescence intensity of SQDs almost unchanged.

3.4. Performance of Apt-SQDs for Hg^{2+} detection

Fig. 4A shows the fluorescence spectra recorded after adding Hg^{2+} solutions with different concentrations (10^{-15} to 10^{-7} M) to Apt-SQDs (1 mg mL^{-1} , pH = 7.4 in PBS). The fluorescence signal of Apt-SQDs decreased gradually with the addition of increasing Hg^{2+} concentrations. The quantitative curves for different concentrations of Hg^{2+} were obtained under certain conditions. Corresponding standard curves were prepared according to the degree of fluorescence quenching, as shown in Fig. 4B. When the Hg^{2+} concentration ranged from 10^{-15} to 10^{-7} M , the linear equation was $\Delta I = 419.8 \lg c(\text{Hg}^{2+}) + 7268$ ($R^2 = 0.9956$) with a low limit of detection (LOD) of 0.3 fM, indicating the effective detection of Hg^{2+} at ultralow concentrations ($\Delta I = F_0 - F$, where F_0 represents the initial fluorescence intensity and F represents the fluorescence intensity after adding Hg^{2+}). In order to further prove the sensitivity of Apt-SQDs to Hg^{2+} , the fluorescence spectra for NH_2 -SQDs detecting various concentrations of Hg^{2+} was supplemented, as shown in Fig. S9. By comparison with Fig. 4, it can be clearly seen that the sensitivity of Apt-SQDs is better than NH_2 -SQDs. Meanwhile, we speculate that Apt-SQDs has better selectivity to Hg^{2+} than NH_2 -SQDs. In addition, Table S1 summarizes the performance of several existing Hg^{2+} sensors and reported detection methods in terms of

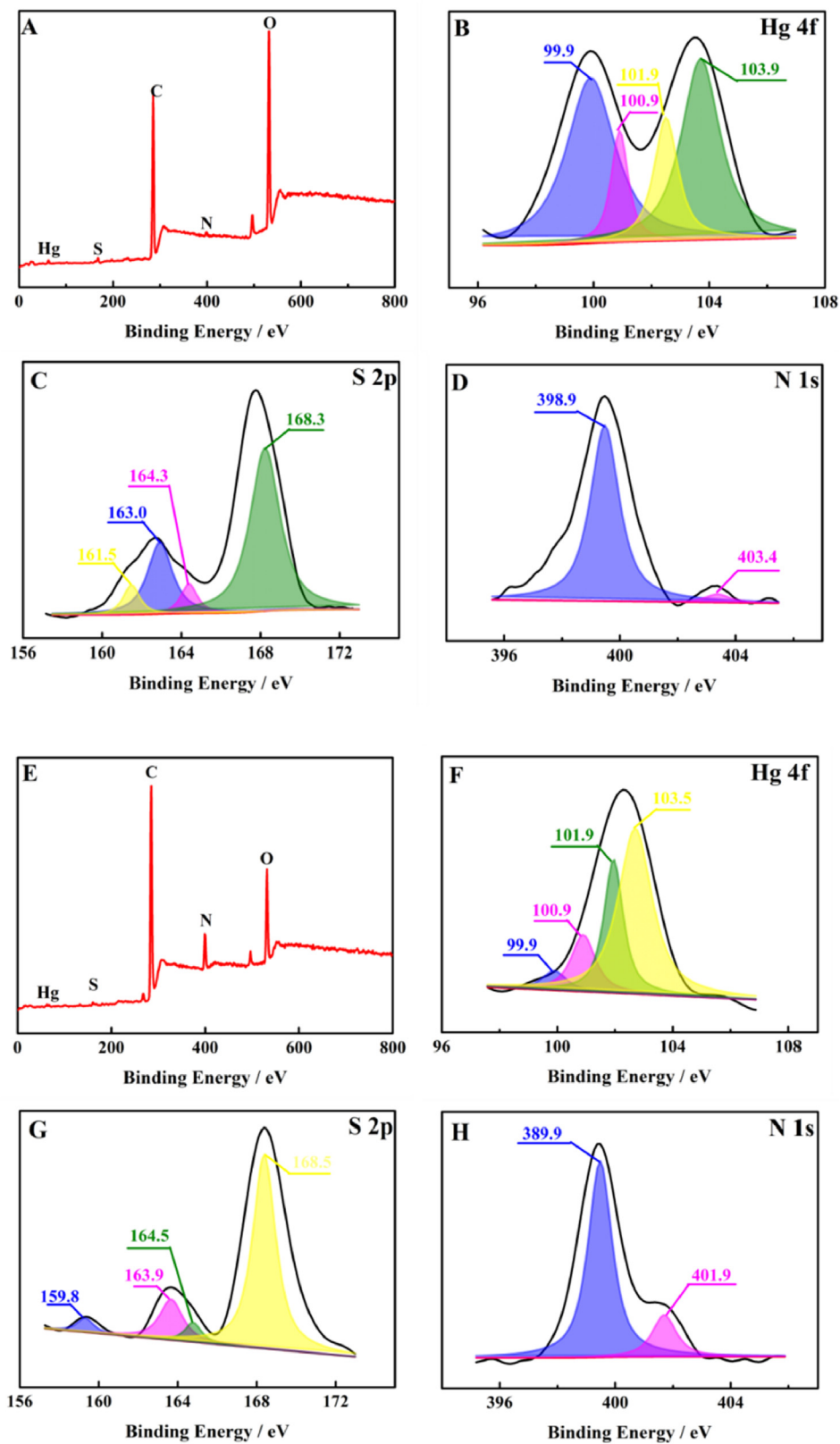


Fig. 3 XPS results for (A) $\text{NH}_2\text{-SQDs} + \text{Hg}^{2+}$ and high-resolution (B) Hg 4f, (C) S 2p, (D) N 1s spectra. XPS results for (E) $\text{Apt-SQDs} + \text{Hg}^{2+}$ and high-resolution (F) Hg 4f, (G) S 2p, (H) N 1s spectra.

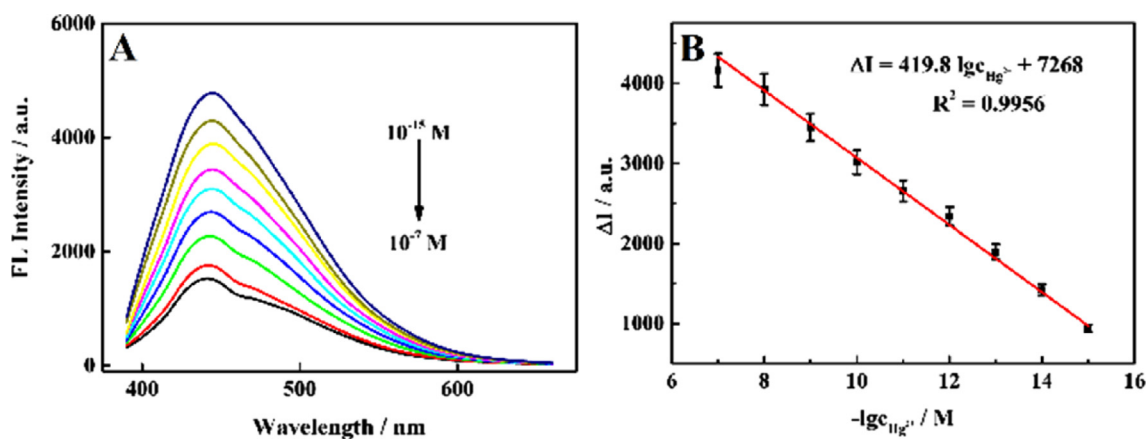


Fig. 4 (A) The signal response of the proposed fluorescent aptasensor for detecting various concentrations of Hg^{2+} and the corresponding concentrations of Hg^{2+} (10^{-15} , 10^{-14} , 10^{-13} , 10^{-12} , 10^{-11} , 10^{-10} , 10^{-9} , 10^{-8} and 10^{-7} M, from top to bottom, $n = 8$). (B) Linear relationship between the fluorescence intensity and the logarithm of Hg^{2+} concentrations.

the LOD and detection range. Compared with other methods, the sensor platform had a lower LOD and a wider detection range, which met the increasingly rigorous requirements for real sample detection. Table S2 summarizes the detection methods of Hg^{2+} based on CQDs. It can be seen from the table that our material sensitivity and detection range are far superior to previous reports. To get insight into the fluorescence quenching mechanism involved, the fluorescence quenching data were analyzed by the Stern-Volmer equation and K_{SV} is the Stern-Volmer constant. As shown in Fig. S10, the Stern-Volmer plot does not fit a conventional linear Stern-Volmer equation, indicating both dynamic and static quenching processes occur in this sensor system.

The good selectivity of the sensor platform based on Apt-SQDs was a prerequisite for practical application. The interference of other ions must be eliminated to accurately determine the content of Hg^{2+} in real samples. Fig. 5A shows the response of the sensing platform to Hg^{2+} and other heavy metal ions under the same conditions, and the degree of fluorescence quenching was recorded. With the exception of Hg^{2+} , other heavy metal ions had little effect on the fluorescence intensity of the sensing platform, which was mainly attributed to the high selectivity of the T- Hg^{2+} -T structure for Hg^{2+} . Common anions were further tested for interference with the

probe, as shown in Fig. S11, indicating that the prepared probe has good selectivity. Furthermore, reproducibility of the sensing platform was also important. Five groups of Apt-SQDs were prepared under the same conditions to construct the fluorescence sensing platform and test fluorescence performance (Fig. 5B). The fluorescence performance of the fluorescence sensing platform based on the five groups of Apt-SQDs was almost identical, and thus the reproducibility of the sensor platform was good. In addition, good stability was one of the important factors determining the feasibility of this sensing platform. Therefore, within two weeks, the same batch of sensing platforms constructed from Apt-SQDs was tested to determine the fluorescence stability under the same experimental conditions, and the results are shown in Fig. 5C. The experimental results indicated that the performance of the constructed sensing platform was very stable. Even after two weeks of placement, the fluorescence emission intensity of the sensor platform was approximately the same as that recorded at the beginning of the experiment. Without special instructions, all the above experiments were repeated eight times to obtain accurate results, that means, $n = 8$.

Although our study can achieve sensitive detection of Hg^{2+} , there are still many methods superior to our work due to the limitation of fluorescence detection technology

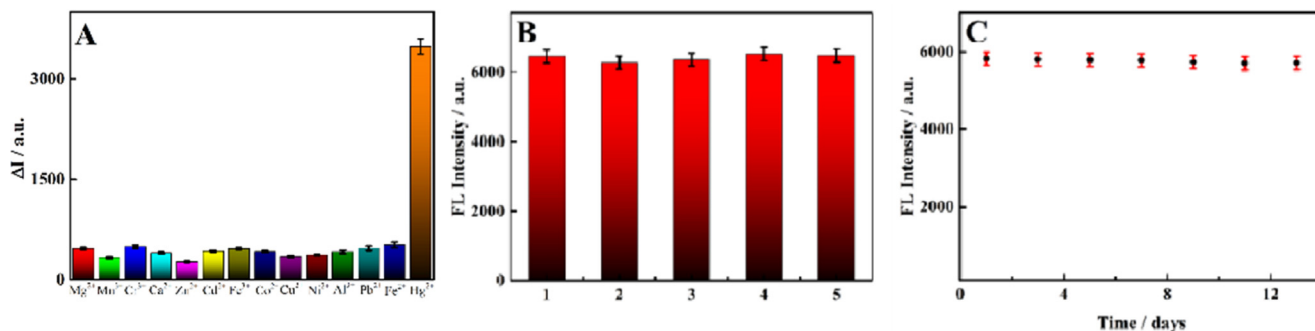


Fig. 5 (A) Selectivity toward other interfering substances in the presence 1.0×10^{-8} M Hg^{2+} : Ca^{2+} , Mg^{2+} , Mn^{2+} , Fe^{3+} , Zn^{2+} , Co^{2+} , Cd^{2+} , Pb^{2+} , Cr^{3+} , Cu^{2+} , Al^{3+} , Ni^{2+} and Fe^{2+} (the concentration of each of the aforementioned interferents was 1.0×10^{-7} M). (B) Reproducibility of the five groups of Apt-SQDs. (C) The fluorescence stability of Apt-SQDs within two weeks ($n = 8$).

Table 1 Hg²⁺ recovery tests in water samples by Apt-SQDs fluorescent aptasensor.

Samples	Added / M	Found / M	Recovery / %	RSD / %
Tap water	0	0	–	–
	10 ⁻⁷	0.9835 × 10 ⁻⁷	98.35	2.1
	10 ⁻¹²	1.073 × 10 ⁻¹²	107.3	1.5
	10 ⁻¹⁵	1.141 × 10 ⁻¹⁵	114.1	3.8
Lake water	0	0	–	–
	10 ⁻⁷	0.9748 × 10 ⁻⁷	97.48	3.6
	10 ⁻¹²	1.038 × 10 ⁻¹²	103.8	1.1
	10 ⁻¹⁵	0.8721 × 10 ⁻¹⁵	87.21	2.9
River water	0	0	–	–
	10 ⁻⁷	1.044 × 10 ⁻⁷	104.4	1.7
	10 ⁻¹²	1.102 × 10 ⁻¹²	110.2	3.4
	10 ⁻¹⁵	0.8937 × 10 ⁻¹⁵	89.37	2.6

and material (Zhang et al., 2020; Rathnakumar et al., 2021., Liu et al., 2021a,b,c; Hasanjani and Zarei, 2018; Babamiri et al., 2018; Zhang et al., 2015).

3.5. Detection of Hg²⁺ concentrations in real samples

With the development of society, the problem of heavy metal pollution has gradually attracted the attention of the public, especially the problem of heavy metal pollution in water. Hg²⁺ was well recognized by the sensing platform. We randomly tested the local water source (Yantai City) as real samples. The concentration of Hg²⁺ was calculated from the standard curve, as shown in Table 1. The recovery rate of Hg²⁺ was 87.21–114.1%, and the relative standard deviation (RSD) was 1.1–3.8%. Therefore, the sensing platform had high accuracy, accuracy and selectivity and was useful for the detection of Hg²⁺ in water samples.

3.6. Portable test papers for Hg²⁺ detection

If Hg²⁺ enters the water environment, it will eventually endanger human health. Therefore, a portable and fast method to monitor Hg²⁺ in environmental water samples must be developed. Fig. S12 clearly shows the quenching of the fluorescence of the test papers to different degrees within 1 min in the presence of different concentrations of Hg²⁺. After an incubation with increasing Hg²⁺ concentrations, the degree of fluorescence quenching gradually increased, consistent with the result of Hg²⁺ detection by the fluorescent aptasensor. Based on this result, the test paper had ultrahigh sensitivity for Hg²⁺ detection, which may be a good qualitative method for Hg²⁺ and had potential application in the safety monitoring of Hg²⁺ in environmental water samples.

4. Conclusions

In this paper, an ultrasensitive dual recognition strategy for detecting Hg²⁺ was successfully developed based on Apt-SQDs. Functionalized SQDs were combined with a variety of groups, which not only ensured the fluorescence performance of functionalized SQDs but also substantially expanded the potential applications of SQDs. The synthesized Apt-SQDs were stable for more than ten days and characterized using many kinds of techniques. Based on the strong binding of S_x²⁻ to Hg²⁺ and the efficient enrichment of T-Hg²⁺-T, a novel fluorescence sensor

for the rapid and ultrasensitive detection of Hg²⁺ was constructed. Apt-SQDs had the advantages of a quick response, high selectivity, low LOD and wide linear range for Hg²⁺ detection. The dual recognition strategy was applied to the detection of Hg²⁺ concentrations in real environmental water samples (tap water, lake and river), with good results and recoveries of 97.39–106.9%. Moreover, the fluorescence quenching effect was obviously observed with the naked eye when trace Hg²⁺ concentrations were detected with portable test papers based on Apt-SQDs. The good performance of Hg²⁺ detection indicated that the method had potential application value in the field monitoring of Hg²⁺ concentrations in environmental water samples.

Declaration of Competing Interest

The authors declare that they have no known competing financial interests or personal relationships that could have appeared to influence the work reported in this paper.

Acknowledgement

The authors gratefully acknowledge the support of the National Natural Science Foundation of China (21778047), and Natural Science Foundation of Shandong Province (grant no. ZR2021MB024).

Appendix A. Supplementary material

Supplementary data to this article can be found online at <https://doi.org/10.1016/j.arabjc.2022.104080>.

References

- Abraham, H.C., Beatriz, E.S.H., Sergio, M., Juan, C.M.L., Edith, G., Francisca, P.S., 2021. Alterations in gene expression due to chronic lead exposure induce behavioral changes. *Neurosci. Biobehav. Rev.* 126, 361–367. <https://doi.org/10.1016/j.neubiorev.2021.03.031>.
- Amico, D., Tassone, A., Pirrone, N., Sprovieri, F., Naccarato, A., 2022. Recent applications and novel strategies for mercury determination in environmental samples using microextraction-based approaches: A review. *J. Hazard. Mater.* 433, <https://doi.org/10.1016/j.jhazmat.2022.128823> 128823.
- Babamiri, B., Salimi, A., Hallaj, R., 2018. Switchable electrochemiluminescence aptasensor coupled with resonance energy transfer for selective attomolar detection of Hg²⁺ via CdTe@CdS/dendrimer

- probe and Au nanoparticle quencher. *Biosens. Bioelectron.* 102, 328–335. <https://doi.org/10.1016/j.bios.2017.11.034>.
- Bader, R.F., 1991. A quantum theory of molecular structure and its applications. *Chem. Rev.* 91, 893–901. <https://doi.org/10.1002/chin.199203324>.
- Bao, X., Wang, S., Gao, B., Li, M., 2019. A novel sulfur quantum dot for the detection of cobalt ions and norfloxacin as a fluorescent “switch”. *Dalton Trans.* 48, 8288–8296. <https://doi.org/10.1039/C9DT01186B>.
- Chen, D.J., Li, S.X., Zheng, F.Y., 2016. Water soluble sulphur quantum dots for selective Ag⁺ sensing based on the ion aggregation-induced photoluminescence enhancement. *Anal. Methods* 8, 632–636. <https://doi.org/10.1039/C5AY02451J>.
- Chiu, T.C., Huang, C.C., 2009. Aptamer-functionalized nano-biosensors. *Sensors* 9, 10356–10388. <https://doi.org/10.3390/s91210356>.
- Daniel, M.Y., María, B.G.G., Agustín, C.G., 2013. Electrochemical determination of mercury: A review. *Talanta* 116, 1091–1104. <https://doi.org/10.1016/j.talanta.2013.07.056>.
- Eto, K., Marumoto, M., Takeya, M., 2010. The pathology of methylmercury poisoning (Minamata disease). *Neuropathology* 30, 471–479. <https://doi.org/10.1111/j.1440-1789.2010.01119.x>.
- Fu, L., Wang, A.W., Xie, K.F., Zhu, J.W., Chen, F., Wang, H.G., Zhang, H.W., Su, W.T., Wang, Z.G., Zhou, C.T., Ruan, S.C., 2020. Electrochemical detection of silver ions by using sulfur quantum dots modified gold electrode. *Sensors and Actuators B-Chemical* 304. <https://doi.org/10.1016/j.snb.2019.127390>
- Guo, X.D., Luo, Q.J., Zheng, N., Wang, H.W., Wang, H., Wen, F., Li, S.L., Wang, J.Q., 2014. Development of an ultrasensitive aptasensor for the detection of aflatoxin B₁. *Biosens. Bioelectron.* 56, 340–344. <https://doi.org/10.1016/j.bios.2014.01.045>.
- Guo, X.R., Huang, J.Z., Wei, Y.B., Zeng, Q., Wang, L.S., 2020. Fast and selective detection of mercury ions in environmental water by paper-based fluorescent sensor using boronic acid functionalized MoS₂ quantum dots. *J. Hazard. Mater.* 381. <https://doi.org/10.1016/j.jhazmat.2019.120969>.
- Han, H., Huang, Q., Hui, L., Zhang, J.Y., 2017. Highly efficient cofactors of Cu²⁺-dependent deoxyribozymes. *Chemistryselect* 2, 3925–3931. <https://doi.org/10.1002/slct.201700424>.
- Hassan, E.M., Derosa, M.C., 2020. Recent advances in cancer early detection and diagnosis: role of nucleic acid based aptasensors. *TrAC-Trends Anal. Chem.* 124. <https://doi.org/10.1016/j.trac.2020.115806>
- Hasanjani, H.R.A., Zarei, K., 2018. An electrochemical sensor for attomolar determination of mercury(II) using DNA/poly-L-methionine-gold nanoparticles/pencil graphite electrode. *Biosens. Bioelectron.* 128, 1–8. <https://doi.org/10.1016/j.bios.2018.12.039>.
- Hino, M., Hamada, N., Tajika, Y., Funayama, T., Morimura, Y., Sakashita, T., Yokota, Y., Fukamoto, K., Mutou, Y., Kobayashi, Y., 2010. Heavy ion irradiation induces autophagy in irradiated C2C12 myoblasts and their bystander cells. *J. Electron Microsc.* 59, 495–501. <https://doi.org/10.1093/jmicro/dfq059>.
- Hu, T., Yan, X., Na, W., Su, X., 2016. Aptamer-based aggregation assay for mercury(II) using gold nanoparticles and fluorescent CdTe quantum dots. *Microchim. Acta* 183, 2131–2137. <https://doi.org/10.1007/s00604-016-1831-6>.
- Kukic, I., Kelleher, S.L., Kiselyov, K., 2014. Zn²⁺ efflux through lysosomal exocytosis prevents Zn²⁺-induced toxicity. *J. Cell Sci.* 127, 3094–3103. <https://doi.org/10.1242/jcs.145318>.
- Li, H., Chen, Q., Hassan, M.M., Jiao, T.H., Xu, Y., Chen, M., 2018. AuNS@Ag core-shell nanocubes grafted with rhodamine for concurrent metal-enhanced fluorescence and surfaced enhanced Raman determination of mercury ions. *Anal. Chim. Acta* 1018, 94–103. <https://doi.org/10.1016/j.aca.2018.01.050>.
- Li, Y., Yang, C., Wang, S., Yang, D., Huang, K., 2020a. Copper and iron ions accelerate the prion-like propagation of α -synuclein: A vicious cycle in Parkinson's disease. *Int. J. Biol. Macromol.* 163, 562–573. <https://doi.org/10.1016/j.ijbiomac.2020.06.274>.
- Li, Y.P., Li, Y.J., Duan, J.L., Hou, J.Y., Hou, Q., Yang, Y.C., Li, H. S., Ai, S.Y., 2020b. Rapid and ultrasensitive detection of mercury ion (II) by colorimetric and SERS method based on silver nanocrystals. *Microchem. J.* 161. <https://doi.org/10.1016/j.microc.2020.105790>
- Liu, C.B., Ye, Z.W., Wei, X.J., Mao, S., 2021a. Recent advances in field-effect transistor sensing strategies for fast and highly efficient analysis of heavy metal ions e2100137 *Electrochem. Sci. Adv.* <https://doi.org/10.1002/elsa.202100137>.
- Liu, J.H., Ma, Z.W., Zhang, D., Guo, J., Li, M., Wang, T.L., Yin, H. Y., 2021b. An anthraquinone-based “turn-on” fluorescence probe for Hg²⁺ detection and its application in cell imaging. *Inorg. Chem. Commun.* 130. <https://doi.org/10.1016/j.inoche.2021.108753>
- Liu, L.X., Ye, K., Lin, C.Q., Jia, Z.Y., Xue, T.Y., Nie, A.M., Cheng, Y.C., Xiang, J.Y., Mu, C.P., Wang, B.C., Wen, F.S., Zhai, K., Zhao, Z.S., Gong, Y.J., Liu, Z.Y., Tian, Y.J., 2021c. Grain-boundary-rich polycrystalline monolayer WS₂ film for attomolar-level Hg²⁺ sensors. *Nat. Commun.* 12, 3870. <https://doi.org/10.1038/s41467-021-24254-x>.
- Lu, D.T., Chen, Z., Li, Y.F., Yang, J., Shuang, S.M., Dong, C., 2015. Determination of mercury(II) by fluorescence using deoxyribonucleic acid stabilized silver nanoclusters. *Anal. Lett.* 48, 281–290. <https://doi.org/10.1080/00032719.2014.940527>.
- Ma, J., Yan, L.L., Chen, B.K., Sun, M.Y., 2018. A novel tetraphenylethene-based fluorescence probe based on the Hg²⁺-promoted deprotection of thioacetal. *Heterocycles* 96, 850–857. <https://doi.org/10.3987/COM-18-13887>.
- Morales, M.E., Servant, G., Ade, C., 2015. Altering genomic integrity: heavy metal exposure promotes transposable element-mediated damage. *Biol. Trace Elem. Res.* 166, 24–33. <https://doi.org/10.1007/s12011-015-0298-3>.
- Ozkan, M., 2011. Determination of mercury and nickel by amperometric biosensor prepared with thermostable lactate dehydrogenase. *Trans. Nonferrous Metals Soc. China* 21, 2332–2338. [https://doi.org/10.1016/S1003-6326\(11\)61017-0](https://doi.org/10.1016/S1003-6326(11)61017-0).
- Pasanphan, W., Chirachanchai, S., 2008. Conjugation of gallic acid onto chitosan: An approach for green and water-based antioxidant. *Carbohydr. Polym.* 72, 169–177. <https://doi.org/10.1016/j.carbpol.2007.08.002>.
- Peng, B., Tang, L., Zeng, G.M., Zhou, Y.Y., 2018a. Current progress in aptasensors for heavy metal ions based on photoelectrochemical method: a review. *Curr. Anal. Chem.* 14, 4–12. <https://doi.org/10.2174/1573411013666170412111128>.
- Peng, T., Wang, J.Y., Xie, S.L., Yao, K., Sun, S.J., Zeng, Y.Y., Jiang, H.Y., 2018b. Preparation of protein hybrid fluorescence nanoclusters for rapid detection of mercury ion. *Chin. J. Anal. Chem.* 46, 373–378. <https://doi.org/10.11895/j.issn.0253-3820.170353>.
- Rathnakumar, S., Bhaskar, S., Rai, A., Saikumar, D.V.V., Kambhampati, N.S.V., Sivaramakrishnan, V., Ramamurth, S.S., 2021. Plasmon-coupled silver nanoparticles for mobile phone-based attomolar sensing of mercury ions. *ACS Applied Nano Materials* 4, 8066–8080. <https://doi.org/10.1021/acsnm.1c01347>.
- Shellaiah, M., Sun, K.W., 2021. Progress in metal-organic frameworks facilitated mercury detection and removal. *Chemosensors* 9, 101. <https://doi.org/10.3390/chemosensors9050101>.
- Shi, Y.Q., Li, W.T., Feng, X.P., Lin, L., Nie, P.C., He, Y., 2021. Sensing of mercury ions in Porphyra by Copper@Gold nanoclusters based ratiometric fluorescent aptasensor. *Food Chemistry* 344, 128694. <https://doi.org/10.1016/j.foodchem.2020.128694>.
- Shi, Y.S., Zhang, G.Q., Li, J.J., Zhang, Y., Yu, Y.B., Wei, Q., 2017. Photoelectrochemical determination of Hg(II) via dual signal amplification involving SPR enhancement and a folding-based DNA probe. *Microchim. Acta* 184, 1379–1387. <https://doi.org/10.1007/s00604-017-2141-3>.
- Sugio, T., Komoda, T., Okazaki, Y., Takeuchi, F., 2010. Volatilization of Metal Mercury from Organomercurials by Highly Mercury-

- Resistant *Acidithiobacillus ferrooxidans* MON-1. *Biosci. Biotechnol. Biochem.* 74, 1007–1012. <https://doi.org/10.1271/bbb.90888>.
- Tabaraki, R., Rahmatinya, Z., 2021. Bifunctional nitrogen and fluorine Co-doped carbon dots as fluorescence probe for silicon and mercury by pH switching. *Journal of Fluorescence* 31, 881–887. <https://doi.org/10.1007/s10895-021-02709-0>.
- Takeda, A., Fujii, H., Minamino, T., Tamano, H., 2014. Intracellular Zn²⁺ signaling in cognition. *J. Neurosci. Res.* 92, 819–824. <https://doi.org/10.1002/jnr.23385>.
- Tamás, L., Zelinová, V., 2017. Mitochondrial complex II-derived superoxide is the primary source of mercury toxicity in barley root tip. *J. Plant Physiol.* 209, 68–75. <https://doi.org/10.1016/j.jplph.2016.10.014>.
- Taylor, C.M., Emond, A.M., Lingam, R., Golding, J., 2018. Prenatal lead, cadmium and mercury exposure and associations with motor skills at age 7years in a UK observational birth cohort. *Environ. Int.* 117, 40–47. <https://doi.org/10.1016/j.envint.2018.04.032>.
- Wang, H.G., Wang, Z.G., Xiong, Y., Kershaw, S.V., Li, T.Z., Wang, Y., Zhai, Y.Q., Rogach, A.L., 2019. Hydrogen Peroxide Assisted Synthesis of Highly Luminescent Sulfur Quantum Dots. *Angew. Chem.-Int. Ed.* 58, 7040–7044. <https://doi.org/10.1002/ange.201902344>.
- Xu, S.F., Chen, L.X., Li, J.H., Guan, Y.F., Lu, H.Z., 2012. Novel Hg²⁺-imprinted polymers based on thymine–Hg²⁺–thymine interaction for highly selective preconcentration of Hg²⁺ in water samples. *J. Hazard. Mater.* 237, 347–354. <https://doi.org/10.1016/j.jhazmat.2012.08.058>.
- Yerga, D.M., García, M.B.G., García, A.C., 2013. Electrochemical determination of mercury: A review. *Talanta* 116, 1091–1104. <https://doi.org/10.1016/j.talanta.2013.07.056>.
- Yuan, Z.H., Yang, Y.S., Lv, P.C., Zhu, H.L., 2022. Recent progress in small-molecule fluorescent probes for detecting mercury ions. *Crit. Rev. Anal. Chem.* 52, 250–274. <https://doi.org/10.1080/10408347.2020.1797466>.
- Zhang, X.A., Jiang, Y.J., Zhu, M.C., Xu, Y.W., Guo, Z.M., Shi, J.Y., Han, E., Zou, X.B., Wang, D., 2020. Electrochemical DNA sensor for inorganic mercury(II) ion at attomolar level in dairy product using Cu(II)-anchored metal-organic framework as mimetic catalyst. *Chem. Eng. J.* 383, <https://doi.org/10.1016/j.ccej.2019.123182>.
- Zhang, X.P., Ding, B.M., Wu, H.W., Wang, J.J., Yang, H.L., 2017. A label-free “turn-on” fluorescence method for detecting mercury ion in aqueous solution based on n-methyl mesoporphyrin IX (NMM)/G-quadruplex DNA. *Anal. Sci.* 33, 165–169. <https://doi.org/10.2116/analsci.33.165>.
- Zhang, Y., Zeng, G.M., Tang, L., Chen, J., Zhu, Y., He, X.X., He, Y., 2015. Electrochemical sensor based on electrodeposited graphene-Au modified electrode and nanoAu carrier amplified signal strategy for attomolar mercury detection. *Anal. Chem.* 87, 989–996. <https://doi.org/10.1021/ac503472p>.
- Zhao, Z., Zhou, X., 2012. Ultrasensitive electrochemiluminescence detection of mercury ions based on DNA oligonucleotides and cysteamine modified gold nanoparticles probes. *Sensors Actuators B-Chem.* 171, 860–865. <https://doi.org/10.1016/j.snb.2012.05.084>.
- Zhou, Y.B., Mahapatra, C., Chen, H.Z., Peng, X.S., Ramakrishna, S., Nanda, H.S., 2019. Recent developments in fluorescent aptasensors for the detection of antibiotics. *Current Opin. Biomed. Eng.* 13, 16–24. <https://doi.org/10.1016/j.cobme.2019.08.003>.